

Original Research Article

Catalytic and antibacterial activity of annealed nickel sulfides quantum dotsMuhammad Ikrama^{1*}, Sawaira Moeen¹, Ali Haider², Anwar Ul-Hamid³¹ Solar Cell Applications Research Lab, Department of Physics, Government College University Lahore, Lahore, 54000, Punjab, Pakistan² Department of Clinical Sciences, Faculty of Veterinary and Animal Sciences, Muhammad Nawaz Shareef, University of Agriculture, 66000, Multan, Punjab, Pakistan³ Core Research Facilities, King Fahd University of Petroleum & Minerals, Dhahran, 31261, Saudi Arabia

*Corresponding Author: dr.muhammadikram@gcu.edu.pk

Abstract: In this research, nickel sulfide (NiS) quantum dots (QDs) were prepared through the co-precipitation method and annealed at same temperature with different time. This study aimed to check the influence of annealing time on catalytic reduction of rhodamine B (*RhB*) and antibacterial efficacy against *E. coli*. The synthesized NiS were characterized thorough XRD, UV-Vis, SAED and TEM analysis to check the effect of annealing time on structural, optical and morphological of QDs. XRD spectra depicted that crystallinity of the NiS increased upon enhancing the annealing time. Electronic transition spectroscopy exhibited the blue shift by increasing annealing time, leading to band gap energy enhancement. TEM images demonstrated that agglomeration of the QDs increased by increasing the annealing time. EDS spectra verified the formation of NiS QDs. SAED analysis confirmed the polycrystalline behavior of host and annealed NiS. The pure NiS demonstrated substantial catalytic reduction of *RhB* dye in acidic medium comparison to other media. Moreover, host sample (NiS) exhibited maximum inhibition zone for *E. coli* at higher concentration.

Keywords: NiS, Annealing; QDs, Co-precipitation.

1. Introduction

The fast expansion of industrial sector and the economy has resulted in the emergence of a number of significant problems on a worldwide scale. Polluted water poses a threat to both human health and the natural environment^[1]. Approximately 4 million deaths a year worldwide are attributed to illnesses that are spread by water^[2-4]. Wastewater from sectors such as paper, plastic, and mineral handling contain a broad diversity of artificial dyestuffs, which are the principal cause of pollution in aquatic environments^[5]. Major health and environmental concerns for both people and animals include allergic reactions, skin sensitivity, and liver malfunction^[6]. About forty percent of the colors used in industrial processes are carcinogenic and/or toxic. *RhB* is a cationic dye that is extremely hazardous to human health and considered one of the most damaging dyes overall. *RhB* has widespread application across a variety of industrial sectors, particularly in the textile industry^[7-10]. Recently, researchers have discovered that it has become progressively tough to eliminate colors from water that has been tainted^[11]. Catalysis, carbon filtration, photocatalysis, chemical precipitation, and chlorination are just a few of the many processes utilized in removing colors from water^[12-15]. Catalysis is a process that is both cost-effective and energy-efficient, in addition to being ecologically sustainable^[16]. Infectious mastitis places a significant financial strain on the dairy industry. Mastitis is an infection that can be produced by a diversity of pathogens, including bacteria and fungi. This condition is associated with a variety of changes, including chemical, microbiological, and physical alterations in the milk, as well as clinical abnormalities in the

tissues of the mammary gland^[17,18]. The most common bacteria associated with mastitis are staphylococcus aureus, coliform, and *E. coli*^[19,20]

Among transition metal sulfides, nickel sulfide (NiS) has garnered extensive attention due to its affordable price, outstanding electrical conductivity, distinctive characteristics, high capability to recover light absorption, plentiful active site, broad applications in catalysis, and antimicrobial activity^[21,22]. Recent studies have shown that combining Ni with a non-metal, such as sulfur, improves photocatalytic efficiency^[23]. This is because the high electronegativity of sulfur results in a reduction in the recombination of electron-hole pairs, which in turn leads to improved efficiency. NiS nanomaterials with a variety of morphologies, such as QDs, nanoparticles, nanosheets, and nanorods, have been considered as suitable semiconducting materials for use in catalytic activities because to the fact that they are less poisonous and produce less cast^[24–26]. S. Muninathan et al. synthesized NiS decorated GO amido black 10 B dye 90% under the visible light^[23]. Subbiah Thirumaran et al. prepared iron-nickel sulfide for the degradation of methylene blue and rhodamine B^[27]. Yuan et al. employed a hydrothermal method for the deposition of NiS₂ on CdLa₂S₄ nanocrystals. The as-prepared NiS₂/CdLa₂S₄ photocatalyst achieved three times as high hydrogen evolution rate as the original CdLa₂S₄^[28]. Sajjad Haider used co-precipitation method for synthesis of NiS/CNTs for photocatalytic degradation of methylene blue above 96%^[29].

In order to evaluate the material's capacity to kill bacteria and to degrade organic dyes in contaminated water, the purpose of this research is to first synthesis NiS by making use of a co-precipitation approach that is kind to the environment, and then to evaluate the efficacy of the material in doing so. For a more in-depth look of the synthesized NiS, a variety of different approaches for characterizing them were used. Tests of catalytic activity (CA) were carried out for the purpose of *RhB* dye degradation. In addition, pathogens such as Staphylococcus aureus *Escherichia coli* (*E. coli*) were utilized to investigate the possibility of antibacterial activity in the compound.

2. Experimental section

2.1 Materials

Nickel nitrate hexahydrate [Ni(NO₃)₂·6H₂O], sodium thiosulfate pentahydrate (Na₂S₂O₃·5H₂O) and NaOH were procured from Sigma Aldrich.

2.2 Synthesis of annealed NiS

For synthesis of NiS QDs, Ni(NO₃)₂·6H₂O and Na₂S₂O₃·5H₂O with (2:1) molar ratio were prepared at vigorous agitation for 40 min. 1M precipitating agent (NaOH) was pipetted in above solution to conserve the pH~10. The solution was centrifuged at 8000 *rpm* to eliminate the contaminants and dried at 160°C to attain powder (Figure 1). The prepared NiS was annealed at 300°C for 12 and 24 h. The NiS named as S1, and annealed NiS at 12 and 24 h named as S2 and S2 in the whole manuscript.

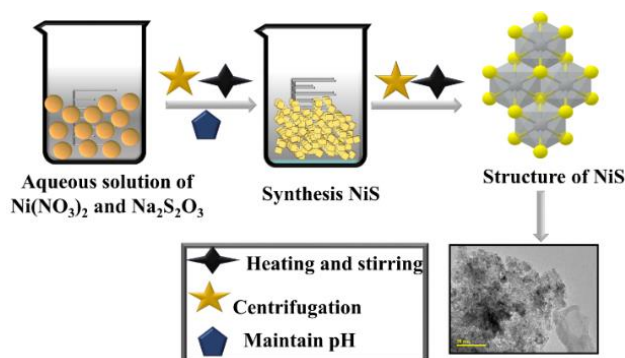


Figure 1 Synthesis of NiS QDs

2.3 Catalytic activity

The ability of *RhB* to degrade in the company of NaBH_4 (reducing agent) and the newly manufactured nano-catalyst (NiS) was evaluated by CA measurements. In its reduced form, *RhB* is colorless, but in its oxidized form, it is pink. A 0.1 M NaBH_4 (reducing agent) solution was dissolved in 3 mL of *RhB* by a quartz cell. In addition, an aqueous solution of *RhB* had 400 microliters of NS solution that had been produced added to it. At room temperature, spectrophotometric tracking of the course of the absorption process was carried out. In the presence of NaBH_4 , *RhB* transformed into *LRhB*, providing evidence that the dyes were degraded. The term “blank” is used to refer to samples that did not contain a nano-catalyst.

2.3.1 Mechanism

In Figure 2, incorporating a nano-catalyst (NiS) and reducing agent to the *RhB* dye is the main catalysis mechanism component. The chemical component contributes one electron to the current reaction and is hence mentioned to as the reducing agent. An e^- from the decreasing agent makes *RhB* an oxidizing agent in a chemical process. During the course of CA, the redox reaction takes place, and it entails the movement of an electron from the acceptor of an oxidant to the reductant. This ultimately results in electron absorption in *RhB*, which in turn causes the synthetic dye to degrade. In addition, MB was examined when a reductant (NaBH_4) was present; nevertheless, the oxidation reaction was extremely sluggish and laborious. The supplement of host and annealed NiS into redox reaction processes serves as an electron convey and enables the transportation of e^- from the BH_4^- to the *RhB*. This helps to circumvent the problems that have been identified. When NSs are used, the adsorption of BH_4^- ions and dye molecules is enhanced, and a high number of active sites urge the ions and molecules to react with each other more quickly, which results in effective degradation of the dye. The effectiveness of the degradation process is improved by the co-existence of a nano-catalyst and a reducing agent. According to what was said before, the dye degradation process in this study utilized a catalytic approach that made use of reducing agents and nano-catalysts^[30–32].

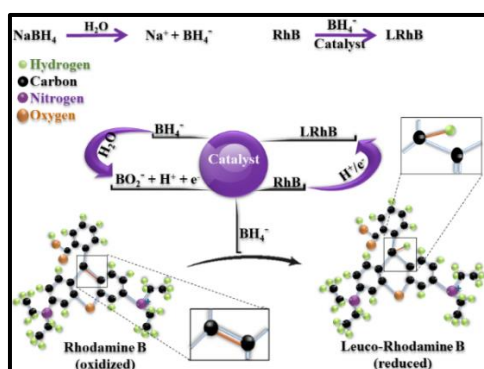


Figure 2 Catalytic mechanism of synthesized catalyst

2.4 Segregation and identification of *E. coli*

The raw milk samples were obtained from several nursing cows at veterinary facilities in Punjab, Pakistan, and placed straight into sterile glassware before being transported to the laboratory at a temperature of 4 degrees Celsius. MacConkey agar (MCA) was used to do an enumeration of the raw milk's associated microorganisms. Incubation took place at 37 degrees Celsius for forty-eight hours in each petri dish.

2.5 Antimicrobial activity

The agar well diffusion method was utilized in order for us to evaluate the antibacterial effectiveness of both bare and annealed NiS in relation to isolated Gram-negative bacteria. After placing MCA on Petri plates, the plates were swabbed with G-negative cultured bacteria (1.5×10^8 CFU mL^{-1}), and a hole measuring 6 millimeters in width was drilled into the cork using a cork borer that had been sanitized. We utilized host and annealed NiS QDs at various doses of 0.5 mg/50 μL and 1 mg/50 μL . These deliberations of NiS were chosen to act as -ve and +ve controls, in contrast to DI water and ciprofloxacin, respectively. The Petri plates were laden

with both minimal and maximal amount of the prepared NiS, and then put in the incubator for 24 hours at 37°C to assess their bactericidal efficiency. A Vernier caliper was utilized to quantify the area of the inhibitory zones^[33,34].

3. Results and discussion

The crystallinity of the samples were determined through XRD spectra in 2θ range from 20 to 65° (Figure 3a). Diffraction peaks at 30.3° (101), 35.0° (021), 40.4° (211) and 48.8°(131) correspond to rhombohedral structure of NiS with space group P63/mmc (JCPDS card no. 012-0041). Peaks at 45.4° (102) and 53.0° (110) attributed to hexagonal phase of NiS (JCPDS card no. 065-0395). Additional peak at 22.0° ($\bar{1}10$) assigned to anorthic structure of NiS₂ described by JCPDS card no. 01-073-0574. Upon enhancing the annealing time of NiS, slight shifting of peaks to smaller angle was observed represents the decrement in lattice strain upon increasing the annealing times. As annealing time increased, crystallinity of the NiS increased as reported by literature^[35]. Additionally, SAED analysis verified the polycrystalline behavior of NiS related to (101), (110), (021) and (102) planes of XRD (Figure 3c-e). The optical features of bare and annealed NiS were determined through electronic transition spectroscopy (Figure 3b). The absorption peak of NiS detected at 273 nm assigned to $n-\sigma^*$ transition [36,37]. Upon increasing the annealing time, hypsochromic shift occurred led to enhancement in band gap energy of NiS.

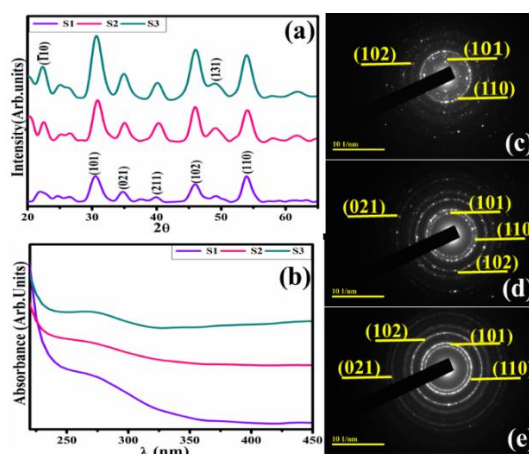
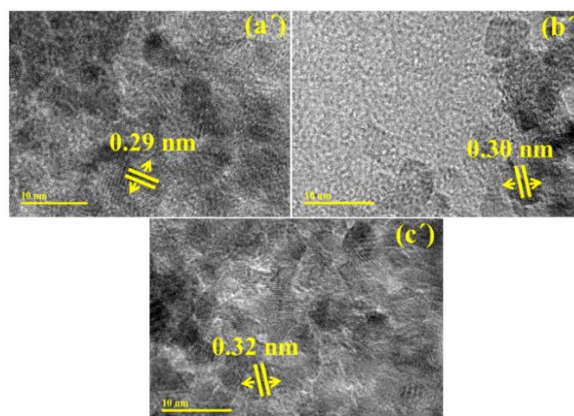


Figure 3 (a) XRD, (b) UV-Vis, (c) SAED analysis of host and annealed NiS (samples S1, S2 and S3)

The morphological and topological characteristics of host and annealed NiS were determined through TEM (Figure 4). Figure 4(a) verified the formation of NiS QDs with average particle size is 6.6 nm. Upon increasing the annealing time, QDs seems to be agglomerated and forming the network (with particle size 7.2 nm) that helps in movement of charge carrier (Figure 4b). The agglomeration of QDs was increased by further enhancing the annealing time (Figure 4c). Furthermore, the d-spacing of NiS was 0.29 nm and increased to 0.32 for sample S3 with increasing the annealing time (Figure 4a-c).



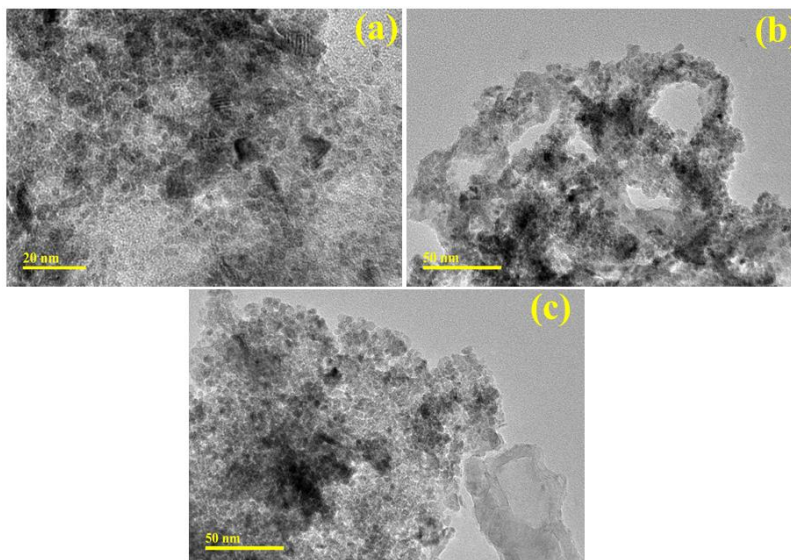


Figure 4 TEM images of samples (a) S1, (b) S2 and (c) S3 and HRTEM images of (a') S1, (b') S2 and (c') S3

The elemental mapping of S3 sample (annealed for 24 h) is shown in Figure 5 (a-f). The occurrence of Ni, S, O and confirmed the synthesis of NiS and sodium (Na) peak occurred due to usage of NaOH (precipitating agent) to conserve the pH during preparation of NiS. The elemental composition of host and annealed NiS were observed by EDS spectra Figure 5(a' -c'). Ni and S peak confirmed the NiS QDs existence.

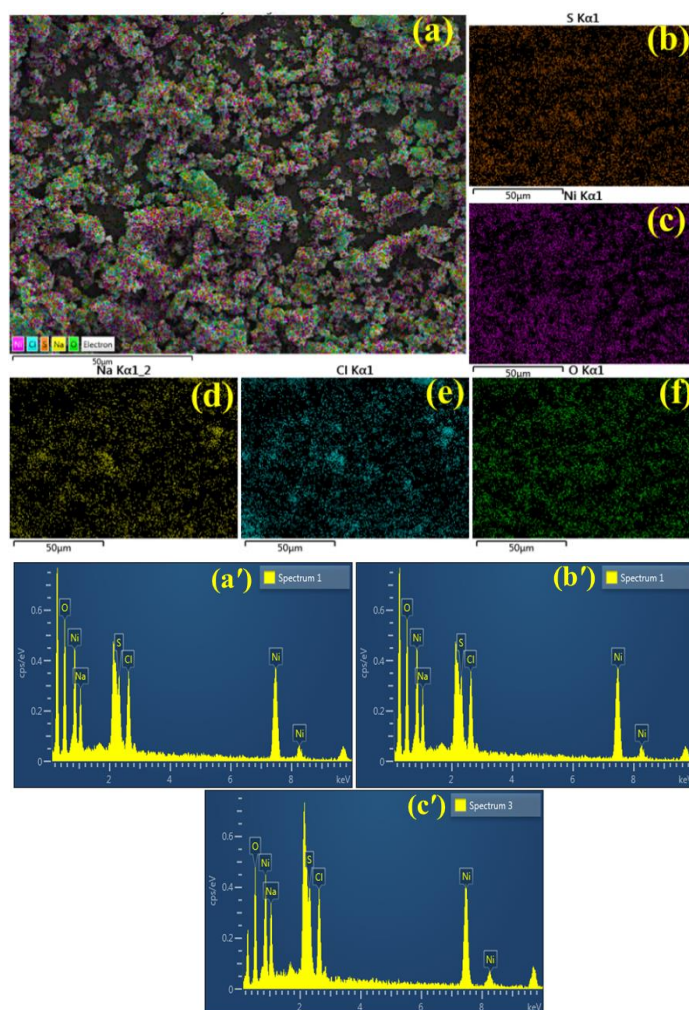


Figure 5(a-e) Mapping of sample S3 (NiS annealed for 24 h) and (a' -c') EDS spectra of S1, S2 and S3

A UV-Vis spectrophotometer was utilized in order to look at the decrease of *RhB* that occurred during CA of annealed NiS₂ QDs. The annealed showed a maximum de-colorization of *RhB* that was 88.7, 60.1 and 42 % in acidic, 59.1, 56.8 and 50.9 % in basic, and 78.7, 75.1 and 62.5 % in a neutral environment, respectively (Figure 7a-c). Due to the increase in the size of the QDs, which supplied a tiny surface area, the *RhB* reduction was lowered as a result of an increase in the annealing time. The crystallinity, pH, and surface area of annealed QDs all have a role in determining the CA^[38,39]. The considerable production of H⁺ ions on the surface of QDs is credited with being the cause of the highest de-colorization of *RhB* that occurred in an acidic solution for sample S1. While under basic circumstances, due to interaction between cationic *RhB* and anionically charged catalyst (NiS), the surface of produced QDs becomes negatively charged, demonstrating strong catalytic effects^[40,41].

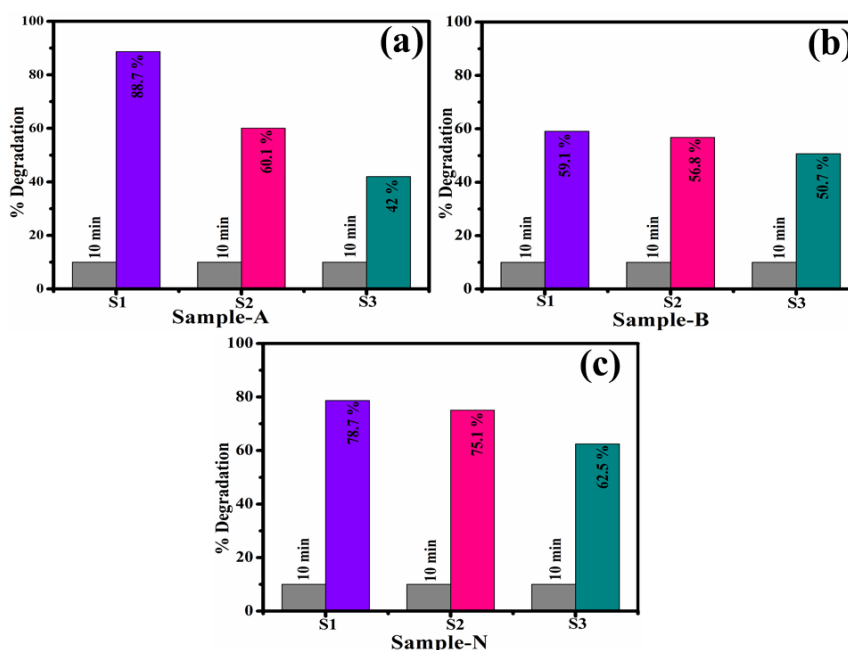


Figure 7 Catalytic activity of samples S1, S2 and S3 in (a) acidic, (b) basic and (c) neutral media

Figure 8 illustrates the antibacterial activity of the produced NiS QDs, which can be found summarized in Table 1. When tested against *E. coli*, the inhibition zone was determined at (3.05-4.95 mm) and (4.45-5.65 mm) at both the minimum and maximum dosages. The findings were contrasted with those of ciprofloxacin (7.25 mm) and deionized water (0 mm). According to the published research^[42], the antibacterial activity of NiS was able to be improved by lengthening the annealing process. Either the NiS₂ QDs interacted with the membrane of the *E. coli* cell or they were transported inside the cell via a bacterial process. The presence of NiS results in the production of reactive oxygen species (ROS), which interface with the cell membrane. This makes it possible for O₂ molecules to interact with iron and cysteine protein within the cell, which in turn causes damage to the DNA of *E. coli* as well as the cell walls^[43].

Table 1 Antibacterial results of pure and annealed NiS

Samples	<i>E. coli</i> Inhibition zone (mm)	
	0.5 mg/50 μ L	1.0 mg/50 μ L
S1	3.05	4.45
S2	4.35	4.90
S3	4.95	5.65
Ciprofloxacin	7.25	7.25
Deionized water (DI)	0.00	0.00

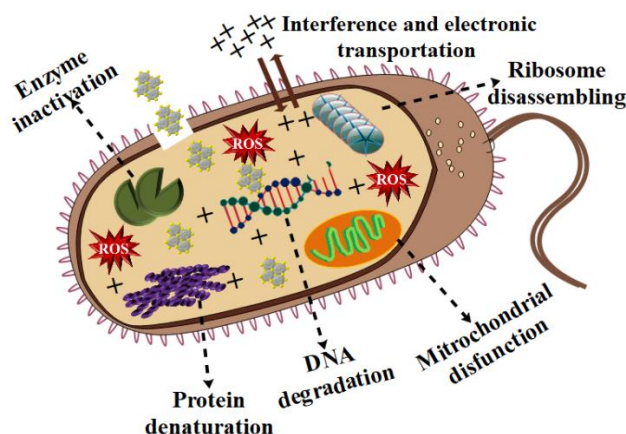


Figure 8 Antibacterial mechanism of synthesized NiS

4. Conclusion

In this work, annealed NiS QDs were effectively prepared through co-precipitation for catalytic decolorization of *RhB* and antibacterial behavior against *E. coli*. TEM demonstrated that the particle size of NiS was 6.6 nm and enhanced to 7.1 nm after annealing. XRD spectra of NiS revealed that crystallinity was improved by annealing the QDs at 300 °C for 12 and 24 h. UV-Vis spectra depicted blue shift after annealing the NiS at 300 °C. Pure NiS exhibited 88.7, 59.1 and 78.7% degradation of *RhB* in acidic, basic and neutral media. While reduction of *RhB* dye decreased from 88.7 to 40% in acidic medium by increasing the annealing time. NiS revealed 3.05 and 4.45 mm inhibition area for *E. coli* at minimal and high concentration. And this inhibition zone increased to 5.65 mm by enhancing the annealing time of NiS.

Acknowledgments

The authors are thankful to higher education commission (HEC), Pakistan through NRPU-20-17615 (M. Ikram).

Data availability

Data will be available on demand.

Conflict of interest

The authors declare no conflict of interest.

References

1. L. Liu, Z. Chen, J. Zhang, D. Shan, Y. Wu, L. Bai, B. Wang, Treatment of industrial dye wastewater and pharmaceutical residue wastewater by advanced oxidation processes and its combination with nanocatalysts: A review, *J. Water Process Eng.* 42 (2021). <https://doi.org/10.1016/j.jwpe.2021.102122>.
2. S.N. Chattopadhyay, N.C. Pan, Ecofriendly printing of jute fabric with natural dyes and thickener, *J. Nat. Fibers.* 16 (2019) 1077–1088. <https://doi.org/10.1080/15440478.2018.1449161>.
3. J. Zhao, L. Ding, X. Sui, Z. Mao, H. Xu, Y. Zhong, L. Zhang, Z. Chen, B. Wang, Bio-based polymer colorants from nonaqueous reactive dyeing of regenerated cellulose for plastics and textiles, *Carbohydr. Polym.* 206 (2019) 734–741. <https://doi.org/10.1016/j.carbpol.2018.11.056>.
4. N. Minju, G. Jobin, S. Savithri, S. Ananthakumar, Double-Silicate Derived Hybrid Foams for High-Capacity Adsorption of Textile Dye Effluent: Statistical Optimization and Adsorption Studies, *Langmuir.* 35 (2019) 9382–9395. <https://doi.org/10.1021/acs.langmuir.9b00898>.

5. R. Darvishi Cheshmeh Soltani, A.R. Khataee, M. Safari, S.W. Joo, Preparation of bio-silica/chitosan nanocomposite for adsorption of a textile dye in aqueous solutions, *Int. Biodeterior. Biodegrad.* 85 (2013) 383–391. <https://doi.org/10.1016/j.ibiod.2013.09.004>.
6. K.T. Kubra, M.S. Salman, M.N. Hasan, Enhanced toxic dye removal from wastewater using biodegradable polymeric natural adsorbent, *J. Mol. Liq.* 328 (2021). <https://doi.org/10.1016/j.molliq.2021.115468>.
7. H. Veisi, S. Azizi, P.M.-J. of cleaner Production, U. 2018, nanoparticles mediated by *Thymbra spicata* extract and its application as a heterogeneous and recyclable nanocatalyst for catalytic reduction of a variety of ..., Elsevier. (n.d.). https://www.sciencedirect.com/science/article/pii/S0959652617322321?casa_token=UVi7e4gpEJ0AAAAA:fiELAPjZOZ64TMH-9N3TqyTlcrZQQe20WgzLiOWzv7CYhjmJuoR1gi_EX45oJzIUqeTMGMIX8qI (accessed September 3, 2023).
8. H. Veisi, S. Azizi, P. Mohammadi, Green synthesis of the silver nanoparticles mediated by *Thymbra spicata* extract and its application as a heterogeneous and recyclable nanocatalyst for catalytic reduction of a variety of dyes in water, *J. Clean. Prod.* 170 (2018) 1536–1543. <https://doi.org/10.1016/j.jclepro.2017.09.265>.
9. M. Naz, A. Rafiq, M. Ikram, A. Haider, S.O.A. Ahmad, J. Haider, S. Naz, Elimination of dyes by catalytic reduction in the absence of light: A review, *J. Mater. Sci.* 56 (2021) 15572–15608. <https://doi.org/10.1007/s10853-021-06279-1>.
10. Y. Guo, O.A. Zeleke, H. Sun, D.H. Kuo, J. Lin, X. Chen, Catalytic reduction of organic and hexavalent chromium pollutants with highly active bimetal CuBiOS oxysulfide catalyst under dark, *Sep. Purif. Technol.* 242 (2020). <https://doi.org/10.1016/j.seppur.2020.116769>.
11. R. Begum, J. Najeeb, A. Sattar, K. Naseem, A. Irfan, A.G. Al-Sehemi, Z.H. Farooqi, Chemical reduction of methylene blue in the presence of nanocatalysts: A critical review, *Rev. Chem. Eng.* 36 (2020) 749–770. <https://doi.org/10.1515/revce-2018-0047>.
12. P.A. Carneiro, D.P. Oliveira, G.A. Umbuzeiro, M.V.B. Zanoni, Mutagenic activity removal of selected disperse dye by photoelectrocatalytic treatment, *J. Appl. Electrochem.* 40 (2010) 485–492. <https://doi.org/10.1007/s10800-009-0018-9>.
13. L. Ren, G. Zhao, L. Pan, B. Chen, Y. Chen, Q. Zhang, X. Xiao, W. Xu, Efficient Removal of Dye from Wastewater without Selectivity Using Activated Carbon- *Juncus effusus* Porous Fibril Composites, *ACS Appl. Mater. Interfaces.* 13 (2021) 19176–19186. <https://doi.org/10.1021/acsami.0c22104>.
14. F. Zaviska, P. Drogui, J.F. Blais, G. Mercier, In situ active chlorine generation for the treatment of dye-containing effluents, *J. Appl. Electrochem.* 39 (2009) 2397–2408. <https://doi.org/10.1007/s10800-009-9927-x>.
15. F. Azeez, E. Al-Hetlani, M. Arafa, Y. Abdelmonem, A.A. Nazeer, M.O. Amin, M. Madkour, The effect of surface charge on photocatalytic degradation of methylene blue dye using chargeable titania nanoparticles, *Sci. Rep.* 8 (2018). <https://doi.org/10.1038/s41598-018-25673-5>.
16. J. Hassan, M. Ikram, A. Ul-Hamid, M. Imran, M. Aqeel, S. Ali, Application of Chemically Exfoliated Boron Nitride Nanosheets Doped with Co to Remove Organic Pollutants Rapidly from Textile Water, *Nanoscale Res. Lett.* 15 (2020). <https://doi.org/10.1186/s11671-020-03315-y>.
17. F.D.-J. of dairy science, U. 1983, Mastitis—progress on control, Elsevier. (n.d.). <https://www.sciencedirect.com/science/article/pii/S0022030283820050> (accessed September 3, 2023).
18. A. Haider, M. Ijaz, S. Ali, J. Haider, M. Imran, H. Majeed, I. Shahzadi, M.M. Ali, J.A. Khan, M. Ikram, Green Synthesized Phytochemically (*Zingiber officinale* and *Allium sativum*) Reduced Nickel Oxide Nanoparticles Confirmed Bactericidal and Catalytic Potential, *Nanoscale Res. Lett.* 15 (2020). <https://doi.org/10.1186/s11671-020-3283-5>.
19. T.Y. Shin, S.H. Yoo, S. Park, Gold nanotubes with a nanoporous wall: Their ultrathin platinum coating and superior electrocatalytic activity toward methanol oxidation, *Chem. Mater.* 20 (2008) 5682–5686.

<https://doi.org/10.1021/cm800859k>.

20. A. Radoń, A. Drygała, Ł. Hawełek, D. Łukowiec, Structure and optical properties of Fe₃O₄ nanoparticles synthesized by co-precipitation method with different organic modifiers, *Mater. Charact.* 131 (2017) 148–156. <https://doi.org/10.1016/j.matchar.2017.06.034>.
21. G.C. Zhang, J. Zhong, M. Xu, Y. Yang, Y. Li, Z. Fang, S. Tang, D. Yuan, B. Wen, J. Gu, Ternary BiVO₄/NiS/Au nanocomposites with efficient charge separations for enhanced visible light photocatalytic performance, *Chem. Eng. J.* 375 (2019). <https://doi.org/10.1016/j.cej.2019.122093>.
22. X.T. Wang, Y. Li, X.Q. Zhang, J.F. Li, X. Li, C.W. Wang, Design and fabrication of NiS/LaFeO₃ heterostructures for high efficient photodegradation of organic dyes, *Appl. Surf. Sci.* 504 (2020). <https://doi.org/10.1016/j.apsusc.2019.144363>.
23. S. Muninathan, S. Arumugam, Enhanced photocatalytic activities of NiS decorated reduced graphene oxide for hydrogen production and toxic dye degradation under visible light irradiation, *Int. J. Hydrogen Energy.* 46 (2021) 6532–6546. <https://doi.org/10.1016/j.ijhydene.2020.11.178>.
24. S. Yan, K. Wang, F. Zhou, S. Lin, H. Song, Y. Shi, J. Yao, Ultrafine Co:FeS₂/CoS₂ Heterostructure Nanowires for Highly Efficient Hydrogen Evolution Reaction, *ACS Appl. Energy Mater.* 3 (2020) 514–520. <https://doi.org/10.1021/acsaem.9b01769>.
25. H.J. Bai, Z.M. Zhang, J. Gong, Biological synthesis of semiconductor zinc sulfide nanoparticles by immobilized *Rhodobacter sphaeroides*, *Biotechnol. Lett.* 28 (2006) 1135–1139. <https://doi.org/10.1007/s10529-006-9063-1>.
26. M.R. Gao, J. Jiang, S.H. Yu, Solution-based synthesis and design of late transition metal chalcogenide materials for oxygen reduction reaction (ORR), *Small.* 8 (2012) 13–27. <https://doi.org/10.1002/sml.201101573>.
27. S. Thirumaran, G. Gurumoorthy, R. Arulmozhi, S. Ciattini, Synthesis of nickel sulfide and nickel–iron sulfide nanoparticles from nickel dithiocarbamate complexes and their photocatalytic activities, *Appl. Organomet. Chem.* 34 (2020). <https://doi.org/10.1002/aoc.5761>.
28. Y.P. Yuan, S.W. Cao, L.S. Yin, L. Xu, C. Xue, NiS₂ Co-catalyst decoration on CdLa₂S₄ nanocrystals for efficient photocatalytic hydrogen generation under visible light irradiation, *Int. J. Hydrogen Energy.* 38 (2013) 7218–7223. <https://doi.org/10.1016/j.ijhydene.2013.03.169>.
29. S. Haider, S.S. Shar, I. Shakir, P.O. Agboola, Design of NiS/CNTs nanocomposites for visible light driven catalysis and antibacterial activity studies, *Ceram. Int.* 47 (2021) 34269–34277. <https://doi.org/10.1016/j.ceramint.2021.08.337>.
30. O.A. Alani, H.A. Ari, N.A.O. Offiong, S.O. Alani, B. Li, Q. rui Zeng, W. Feng, Catalytic Removal of Selected Textile Dyes Using Zero-Valent Copper Nanoparticles Loaded on Filter Paper–Chitosan–Titanium Oxide Heterogeneous Support, *J. Polym. Environ.* 29 (2021) 2825–2839. <https://doi.org/10.1007/s10924-021-02062-0>.
31. M. Saeed, M. Siddique, M. Ibrahim, N. Akram, M. Usman, M.A. Aleem, A. Baig, *Calotropis gigantea* leaves assisted biosynthesis of ZnO and Ag@ZnO catalysts for degradation of rhodamine B dye in aqueous medium, *Environ. Prog. Sustain. Energy.* 39 (2020). <https://doi.org/10.1002/ep.13408>.
32. K.K. Bera, M. Chakraborty, M. Mondal, S. Banik, S.K. Bhattacharya, Synthesis of α - β Bi₂O₃ heterojunction photocatalyst and evaluation of reaction mechanism for degradation of RhB dye under natural sunlight, *Ceram. Int.* 46 (2020) 7667–7680. <https://doi.org/10.1016/j.ceramint.2019.11.269>.
33. V.M. Pierce, A.J. Mathers, Setting Antimicrobial Susceptibility Testing Breakpoints: A Primer for Pediatric Infectious Diseases Specialists on the Clinical and Laboratory Standards Institute Approach, *J. Pediatric Infect. Dis. Soc.* 11 (2022) 73–80. <https://doi.org/10.1093/jpids/piab106>.
34. B.A. Iwalokun, A. Ogunledun, D.O. Ogbolu, S.B. Bamiro, J. Jimi-Omojola, In vitro antimicrobial properties of aqueous garlic extract against multidrug-resistant bacteria and *Candida* species from Nigeria,

- J. Med. Food. 7 (2004) 327–333. <https://doi.org/10.1089/jmf.2004.7.327>.
35. D. Negi, R. Shyam, S.R. Nelamarri, Role of annealing temperature on structural and optical properties of MgTiO₃ thin films, *Mater. Lett. X.* 11 (2021). <https://doi.org/10.1016/j.mlblux.2021.100088>.
 36. M. Salavati-Niasari, G. Banaiean-Monfared, H. Emadi, M. Enhessari, Synthesis and characterization of nickel sulfide nanoparticles via cyclic microwave radiation, *Comptes Rendus Chim.* 16 (2013) 929–936. <https://doi.org/10.1016/j.crci.2013.01.011>.
 37. K. Skrabania, A. Miasnikova, A.M. Bivigou-Koumba, D. Zehm, A. Laschewsky, Examining the UV-vis absorption of RAFT chain transfer agents and their use for polymer analysis, *Polym. Chem.* 2 (2011) 2074–2083. <https://doi.org/10.1039/c1py00173f>.
 38. S. Munusamy, R. sai laxmi Aparna, R. gunneswara subramanya v Prasad, Photocatalytic effect of TiO₂ and the effect of dopants on degradation of brilliant green, *Sustain. Chem. Process.* 1 (2013). <https://doi.org/10.1186/2043-7129-1-4>.
 39. S. Moeen, M. Ikram, A. Haider, J. Haider, A. Ul-Hamid, W. Nabgan, T. Shujah, M. Naz, I. Shahzadi, Comparative Study of Sonophotocatalytic, Photocatalytic, and Catalytic Activities of Magnesium and Chitosan-Doped Tin Oxide Quantum Dots, *ACS Omega.* 7 (2022) 46428–46439. <https://doi.org/10.1021/acsomega.2c05133>.
 40. Ayesha, M. Imran, A. Haider, I. Shahzadi, S. Moeen, A. Ul-Hamid, W. Nabgan, A. Shahzadi, T. Alshahrani, M. Ikram, Polyvinylpyrrolidone and chitosan-coated magnetite (Fe₃O₄) nanoparticles for catalytic and antimicrobial activity with molecular docking analysis, *J. Environ. Chem. Eng.* 11 (2023). <https://doi.org/10.1016/j.jece.2023.110088>.
 41. M. Ikram, A. Haider, M. Imran, J. Haider, S. Naz, A. Ul-Hamid, A. Shahzadi, K. Ghazanfar, W. Nabgan, S. Moeen, S. Ali, Assessment of catalytic, antimicrobial and molecular docking analysis of starch-grafted polyacrylic acid doped BaO nanostructures, *Int. J. Biol. Macromol.* 230 (2023). <https://doi.org/10.1016/j.ijbiomac.2023.123190>.
 42. A. Mahmoodi, S. Solaymani, M. Amini, N.B. Nezafat, M. Ghoranneviss, Structural, Morphological and Antibacterial Characterization of CuO Nanowires, *Silicon.* 10 (2018) 1427–1431. <https://doi.org/10.1007/s12633-017-9621-2>.
 43. T.U. Doan Thi, T.T. Nguyen, Y.D. Thi, K.H. Ta Thi, B.T. Phan, K.N. Pham, Green synthesis of ZnO nanoparticles using orange fruit peel extract for antibacterial activities, *RSC Adv.* 10 (2020) 23899–23907. <https://doi.org/10.1039/d0ra04926c>.